Pakistan J. Zool., pp 1-15, 2024. **DOI**: https://dx.doi.org/10.17582/journal.pjz/20230817034610

Comparative Transcriptomic and Proteomic Analyses Provide Insights into the Key Genes Involved in Fat Deposition in Diqing Tibetan Pig

Jingru Nie[1,2], Bo Zhang[2], Li Ma[3], Dawei Yan[1], Hao Zhang[2] and Xinxing Dong[1]*

[1]*College of Animal Science and Technology, Yunnan Agricultural University, Kunming 650201, China*
[2]*College of Animal Science and Technology, China Agricultural University, Beijing 100193, China*
[3]*Department of Animal Husbandry and Veterinary Medicine, Yunnan Vocational and Technical College of Agriculture, Kunming 650212, China*

Jingru Nie and Bo Zhang contributed equally to this work.

Article Information
Received 17 August 2023
Revised 05 October 2023
Accepted 21 October 2023
Available online 02 October 2024 (early access)

Authors' Contribution
DY and XD conceived the study. LM performed the experiments. BZ and HZ analyzed the data. JN wrote the manuscript. All authors have read and approved the final version.

Key words
Diqing Tibetan pig, Fat deposition, Proteome, Transcriptome, Differential genes, Differential proteins

ABSTRACT

The contents of subcutaneous, intramuscular, and intermuscular fat directly affect pork quality. The large Diqing Tibetan pig (TP) is a unique plateau pig breed in China. However, the mechanism of transcriptional regulation of fat deposition in this pig is unclear. We aimed to identify the important genes and proteins involved in fat deposition in TPs. We obtained transcriptomic and proteomic data from backfat (BF) tissues of TP and Duroc pigs (DP) via RNA-seq and isobaric tags for relative and absolute quantitation analyses, respectively. Comparative analyses of TP and DP yielded 1,452 differentially expressed genes (DEGs), and 126 differentially abundant proteins (DAPs). Functional annotation of these DEGs and DAPs revealed enrichment in metabolic processes, insulin signaling pathways, fatty acid synthesis, lipid metabolism, pyruvate metabolism, carboxylic acid metabolic processes, and other related pathways. Eleven genes and their encoded proteins (*SCD*, *LPIN1*, *PECR*, *FMO3*, *THRSP*, *SNCG*, *GM2A*, *HK1*, *ADIPOQ*, *PLAAT*, and *NUPR1*) were identified as key candidate regulators that might be crucial in the fat deposition traits of TPs. This study provides reference data for analyses of the genetic regulation mechanism of fat deposition and improved meat quality of TPs using molecular marker-assisted selection.

INTRODUCTION

Pig carcass fat is mainly deposited in subcutaneous, perivisceral, and skeletal muscle tissue. The contents of subcutaneous, intramuscular, and intermuscular fat directly affect pork quality (Hausman *et al*., 2018).

During the growth of pigs, the development and metabolism of adipose tissues in different parts are not consistent. The rapid growth period of subcutaneous fat is the earliest, followed by growth of visceral and intramuscular fat, with the intramuscular fat development being the last stage. The increase in intramuscular fat typically begins after 16 weeks of age. This significant deposition reflects increases in the cell size and number. In contrast to subcutaneous adipose tissue, the number of intramuscular adipocytes does not reach a plateau at 24 weeks of age and continues to increase. With the rapid deposition of intramuscular fat, the activities of malate and citrate lyase in intramuscular adipocytes are increased. Enzyme activity in subcutaneous adipose tissue is greatest at 16 weeks of age and then gradually decreases. Enzyme activity in intramuscular adipose tissue does not decrease before 24 weeks of age, but increases at a decreasing rate after 16 weeks. During lactation, lipoprotein lipase activity in intramuscular fat is high and remains unchanged until 24 weeks of age (Lee and Kauffman, 1974). Monziols *et al*. (2007) found that the intramuscular fat content in pigs was the lowest, the subcutaneous was slightly higher than intramuscular fat content, and the perirenal fat content was the highest. The proportion of unsaturated fatty acids

* Corresponding author: 86127447@qq.com
0030-9923/2023/0001-0001 $ 9.00/0

(FAs) in adipose tissue of different parts showed regular changes from the outer layer of subcutaneous fat to the inner layer, intermuscular fat, and perirenal fat. The ratio of unsaturated FAs/saturated FAs in fat gradually decreased, and the content of monounsaturated FA showed the same trend. The collective findings highlight the marked differences in the fat development sequence, fat synthesis ability, lipid content, and FA composition among different parts of the body.

Subcutaneous fat of livestock accounts for approximately 70% of their total fat. Adipose tissue is mainly composed of adipocytes. Adipocytes are pluripotent mesenchymal stem cells (MSCs) derived from the mesoderm (Lin *et al*., 2010). These cells exist both in the vascular matrix of adipose tissue and bone marrow (Tang and Lane, 2012). Upon stimulation by signaling factors, such as long-term energy or glucose intake, MSCs undergo multiple rounds of mitosis and differentiate into adipocytes. These signaling factors mainly include bone morphogenetic protein 4 (BMP4), BMP2, Wnt, and Hedgehog (Hh) signaling pathways of the BMP family. The BMP4 and BMP2 signaling pathways can promote the adipogenic differentiation of MSCs (Bowers *et al*., 2006). The Hh signaling pathway can inhibit the adipogenic differentiation of MSCs (Spinella-Jaegle *et al*., 2001). The Wnt signaling pathway has different regulatory effects on the adipogenic differentiation of MSCs at different stages. The typical Wnt signaling pathway can promote the adipogenic differentiation of MSCs in the early stage and inhibit peroxisome proliferator-activated receptor gamma (PPARγ) and CCAAT-enhancer-binding protein alpha (C/EBPα) isolipogenic differentiation marker genes in the late adipogenic differentiation of adipocytes, playing a role in inhibiting lipogenesis (Davis and Zur Nieden, 2008).

With the development of high-throughput sequencing technology, several genes and proteins related to fat deposition have been identified. In one study, two groups of Iberian × Landrace crossbred pigs with different intramuscular FA contents were the subjects, with an average slaughtering age of 179.8 ± 2.6 days. Backfat (BF) tissue was analyzed by RNA sequencing (RNA-seq), and the biological pathways of different genes involved in fat and FA metabolism were identified (Corominas *et al*., 2013). In another study, RNA-seq was used to compare and analyze the liver and longissimus dorsi (LD) of Berkshire pig and Jeju native pig. Compared with Berkshire pig, 169 and 39 differentially expressed genes (DEGs) were identified in the liver and LD of Jeju native pig, respectively. The DEGs were significantly enriched in biological processes (BP) and signal pathways related to lipid metabolism (Sodhi *et al*., 2014). Chen *et al*. (2017) analyzed intramuscular fat gene expression patterns of 280-days old Laiwu and large white pigs. DEGs were mainly enriched in the FA anabolic pathway related to fat metabolism. Cardoso *et al*. (2017) determined the differences in the FA composition-related transcripts of skeletal muscle tissue of Duroc pig (DP) by RNA-seq. The authors reported that differential genes were mainly related to lipogenesis, triacylglycerol degradation, and glucose metabolism. By comparing and analyzing the transcriptome data of the subcutaneous and intramuscular adipose tissues of large white pigs, Huang *et al*. (2017) identified 180 DEGs. The upregulated genes were mainly involved in BP related to lipid metabolism, such as cell proliferation, lipid kinase activity, and phospholipid metabolism. Downregulated genes were significantly enrichecd in the mitogen-activated protein kinase (MAPK) signaling pathway, which plays an important role in regulating adipocyte differentiation (Huang *et al*., 2017). In the study by Muñoz *et al*. (2018), Iberian pigs were divided into high and low intramuscular fat groups according to intramuscular fat content. The groups were analyzed by RNA-seq. In animals with a high intramuscular fat content enriched genes related to lipid metabolism included *FASN*, *SCD*, *ELOVL6*, *DAGT2*, *PLIN1*, *CIDEC*, and *ADIPOQ*. In animals with low intramuscular fat content enriched genes related to adipogenesis included *CREB1*, *VDR*, *ATF6*, and *SP1*. Furthermore, the deposition of adipose tissue in pigs varies from breed to breed, and the fat deposition ability of different breeds varies greatly, indicating more pronounced fat deposition in fat-type pigs compared to lean-type pigs (Eggert *et al*., 2007).

Despite this plethora of evidence, the genetic mechanisms underlying fat deposition are not yet fully understood. Developing transcriptomic and proteomic profiles allows for the identification of genes involved in the regulation of fat deposition at mRNA and protein expression levels. Both RNA-seq and isobaric tags for relative and absolute quantitation (iTRAQ) have been widely used to screen functional genes involved in lipid deposition in pigs and other domestic species (Wang *et al*., 2013, 2016). Integrating transcriptome and proteome analyses could provide insights into the key functional genes and their regulatory mechanisms underlying fat deposition in the large Diqing Tibetan pig (TP).

TP is a unique plateau pig breed that can adapt to cold and low-oxygen conditions at high altitudes. They are known for their high-fat deposition and good meat quality. Current research on TPs has mainly focused on their origin and domestication (Yang *et al*., 2011), genetic diversity (Ge *et al*., 2020), and hypoxia adaptation (Jia *et al*., 2016; Wu *et al*., 2020). The transcriptional regulatory mechanism of fat deposition in TPs has not been fully elucidated. DP is a typical lean-type modern breed that is now used for pork

production worldwide. It exhibits high growth rates and lean carcass percentages (Pan *et al*., 2003). Compared with DPs, fat deposition, fat desaturation, and feed utilization of TPs are lower. These differences may be caused by gene and protein expression in BF tissue. Therefore, analysis of DEGs and differentially abundant proteins (DAPs) in the BF tissue between TPs and DPs can be useful in understanding the molecular basis of pig fat deposition.

In this study, we performed a comparative analysis of the transcriptomic and proteomic profiles of BF tissues obtained from TPs and DPs using RNA-seq and iTRAQ technologies to enrich the basic understanding of fat deposition regulation in pigs and other agricultural animals and provide reference data for genetic improvement in TPs.

MATERIALS AND METHODS

Animals and samples

The experimental animals used were domestic pigs that were not endangered or protected. Animal care was in strict accordance with the Guide for the Care and Use of Laboratory Animals in China.

Twelve individuals each of TPs and DPs with the same parity, birth date, and weight were selected for fattening tests at the Tibetan pig breeding farm of the Lvyuan Ecological Breeding Professional Cooperative in Shangri-La city, Yunnan Province, China. The animals were slaughtered at 10 months of age. We selected three pigs with an average weight from each group for BF tissue collection. The extracted tissues were frozen in liquid nitrogen, transported to the laboratory, and stored at -80 °C for the extraction of total RNA and proteins.

RNA isolation, library preparation, and sequencing

Total RNA was isolated using TRIzol® reagent (Invitrogen, Waltham, MA, USA). The integrity, concentration, and purity of each sample were evaluated using 1% agarose gel electrophoresis and a NanoDrop™ 2000 Biophotometer (Thermo Fisher Scientific, Waltham, MA, USA). The samples were reverse-transcribed to cDNA using Superscript II reverse transcriptase (Invitrogen) and random hexamer primers. RNA-seq libraries were constructed according to manuals provided by Illumina Inc. (San Diego, CA, USA) and sequenced using the Illumina HiSeq 2000 platform.

Quality control and alignment of sequencing reads

Raw RNA-seq reads were processed using CLC Genomics Workbench 4.8 software (CLC Bio, Aarhus, Denmark). After removing the adapters, the remaining clean reads were aligned to the whole pig genome (Suscrofa11.1) (ftp://ftp.ensembl.orgpub/release-94/fasta/sus_scrofa/dna/Sus_scrofa.Sscrofa11.1.dna.toplevel.fa.gz) using TopHat software (version 2.0.9) (Trapnell *et al*., 2009). Finally, BAM files generated using SAMtools (Li *et al*., 2009) were used for subsequent analysis. Quality control and read statistics were determined using the FastQC software (http://www.bioinfor-matics.babraham.ac.uk/projects/fastqc/).

Quantification and comparison of gene expression

Fragments per kilobase of exon model per million mapped fragment (FPKM) values obtained using Cufflink software (version 2.1.1) (Trapnell *et al*., 2010) were used to normalize gene expression. Differential expression analyses of the comparison groups (TP vs. DP) were performed using the DESeq R package (1.10.1) (Anders and Huber, 2010). The resulting *P*-values were adjusted using the Benjamini-Hochberg method. The results are expressed as the fold change (FC) of the average expression of the case groups to that of the respective control group. In the comparison group, DEGs were identified as genes with $|\log_2(FC)| > 1$ and $P < 0.05$.

Protein isolation, enzymolysis and iTRAQ labeling

BF tissues in liquid nitrogen were ground to a powder, and each sample was added to lysis buffer (Roche, Basel, Switzerland). The resulting samples were ultrasonically disrupted to extract total protein. Protein concentrations were determined using the BCA protein assay reagent (Beyotime Institute of Biotechnology, Shanghai, China). Protein samples (200 μg) were mixed with dl-dithiothreitol, alkylated with iodoacetamide, and treated with trypsin overnight at a trypsin-to-protein ratio of 1:100. Peptides (15 μg) from each group were labeled using an 8plex iTRAQ reagent multiplex kit (SCIEX, Framingham, MA, USA). The retained peptides were eluted with buffer A (10 mM KH_2PO_4 in 25% acetonitrile, pH 3.0) and buffer B (10 mM KH_2PO_4 and 500 mM KCl in 25% ACN, pH 3.0) at a flow rate of 1.0 mL/min.

Liquid chromatography-tandem mass spectrometry (LC-MS/MS) analysis

Eluted fractions were lyophilized using a centrifugal speed vacuum concentrator (CentriVap® Complete Vacuum Concentrator; Labconco, Kansas City, MO, USA) and dissolved in 0.1% formic acid. Equivalent amounts of peptides from each fraction were subjected to reverse-phase nanoflow LC-MS/MS analysis using the EASY-nLC™ high-performance liquid chromatography system (Thermo Fisher Scientific) connected to a hybrid quadrupole/time-of-flight mass spectrometer equipped with a nano electrospray ion source as described previously

(Michalski *et al*., 2011). The peptides were separated on a C18 analytical reverse-phase column using a mixture of solution A (0.1% formic acid in water) and solution B (0.1% formic acid in acetonitrile). A full MS scan was conducted using a Q Exactive™ mass spectrometer (Thermo Fisher Scientific).

Database search and protein identification and quantification

For peptide identification and quantification, MS/MS data were searched against the X101SC19080936-Z01-Sus_scrofa-ensemble.fasta (45898 sequences) file using Mascot 2.2 and Proteome Discoverer™ 1.4 software (Thermo Fisher Scientific). Unique proteins with at least two unique peptides with a false discovery rate (FDR) < 0.01 (Sandberg *et al*., 2012) were used for further analysis. The final protein ratios were normalized to the median average protein content of the 8plex samples. FC > 1.2 or FC < 0.83 and $P < 0.05$ were the threshold criteria for identifying DAPs.

Functional annotation of DEGs and DAPs

DEGs and DAPs were classified by gene ontology (GO) and kyoto encyclopedia of genes and genomes (KEGG) using database for annotation, visualization and integrated discovery (DAVID) online software (https://david.ncifcrf.gov/). For these analyses, official gene symbols for each DEG or DAP were uploaded and the species with the maximum number of annotations were used. GO terms used were biological process (BP), cellular component (CC), and molecular function (MF). KEGG pathways with corrected $P < 0.05$ were considered significantly enriched. Cytoscape 3.9.0 software (https://apps.cytoscape.org/) was used to mine the interaction relationships between different genes and construct an interaction network diagram of different genes. A protein-protein interaction (PPI) network diagram was constructed, and the interaction relationships were analyzed using the STRING online website (https://string-db.org/).

Verification of important candidate genes

Six candidate genes identified by RNA-seq and iTRAQ were selected for verification by quantitative real-time PCR (qPCR). The qPCR primers designed for the six genes are listed in Table I. qPCR analysis was performed using a SYBR® green I PCR master mix kit (FP204; Tiangen Biotech Co. Ltd., Beijing, China) on a CFX96™ Real-Time PCR Detection System (Bio-Rad, Hercules, CA, USA), according to the manufacturer's instructions. The gene expression levels were calculated using the $2^{-\triangle\triangle Ct}$ method.

Table I. Primers used for the differentially expressed genes.

Genes	Primer sequences (5'-3')	T_m/ °C	Length (bp)
ACACA	F: GGGGTGACTTTCGCACTACA	60	127
	R: GGACGCTCTGCCTGTACTTT		
SREBF1	F: CTGACAAGCTGCCCATCAAC	60	112
	R: GAGCGGTAGCGTTTCTCGAT		
ADIPOQ	F: TTGAAGGTCCCCGAGGTTTC	60	91
	R: CCCACACTGAATGCTGAACG		
PLAAT3	F: CGTTGGCGATGGATATGTGG	59	245
	R: TCAGCTTGTAGAGCACCTCC		
THRSP	F: ACGGAAGGCAGACTCTGTGA	60	159
	R: AAGCATTCTAAAGGCGACCCA		
SCD	F: AAACACCCAGCCGTCAAAGA	60	208
	R: AAGAAAGGTGGCGACGAACA		
GADPH	F: TCGGAGTGAACGGATTTG	60	219
	R: CCTGGAAGATGGTGATGG		

RESULTS

Summary of RNA-seq data

After removing low-quality reads, an average of 46.58 million paired-end reads were obtained for each sample. Of these, approximately 95.61% were mapped to the *Sus scrofa* 11.1 genome sequence (Table II). By calculating the FPKM values for gene expression levels, 10,274 genes were found to be expressed in the BF tissue. Of these, 9,763 were identically expressed in both groups (Fig. 1A). The distributions of FPKM values were similar among the six samples, with no outliers (Fig. 1B).

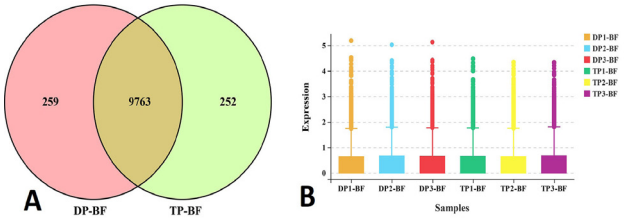

Fig. 1. Distribution of positively expressed genes in porcine backfat tissue. (**A**) Venn diagrams of the number of genes expressed in each group. (**B**) Distributions of expression values of the six samples. The box-and-whisker plots show log10 (FPKM + 1) of each gene from the six sets of RNA-seq data. The line in the box represents the median. The x-axis shows samples, and the y-axis represents gene expression. DP, Duroc pig; TP, large Diqing Tibetan pig; BF, backfat.

Table II. Statistics of RNA-seq data.

Group	Sample	Raw reads number	Clean reads number	Clean reads rate (%)	Mapped reads number	Mapping ratio (%)
DP	D-1BF	48,854,036	45,897,090	93.95	44,050,755	95.98
	D-2BF	51,951,756	47,796,496	92.00	45,804,130	95.83
	D-3BF	50,746,098	47,664,688	93.93	45,781,858	96.05
TP	TP-1BF	50,626,050	47,046,500	92.93	44,765,723	95.15
	TP-2BF	47,769,074	44,977,686	94.16	42,890,387	95.36
	TP-3BF	49,300,214	46,091,332	93.49	43,912,119	95.27

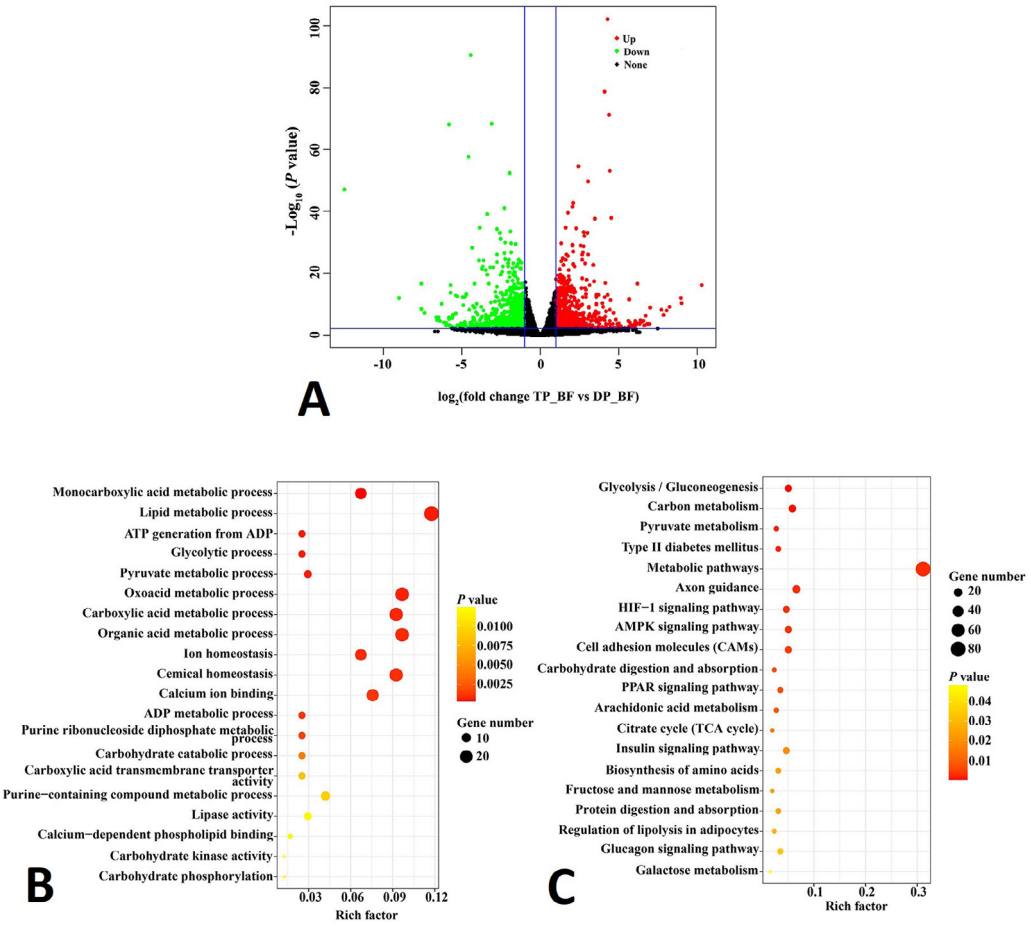

Fig. 2. Identification and functional analysis of DEGs. (**A**) Volcano plot displaying DEGs between TP and DP. Upregulated and downregulated genes are shown in red and green, respectively. Black dots represent genes with similar expression levels. (**B**) GO enrichment analysis of DEGs between TP and DP. The x-axis shows enrichment factor, and the y-axis represents GO enrichment terms. (**C**) KEGG enrichment analysis of DEGs between TP and DP. The x-axis shows enrichment factor, and the y-axis represents KEGG enrichment terms. DEGs, differentially expressed genes; DP, Duroc pig; TP large Diqing Tibetan pig, BF, backfat.

Identification and functional analysis of DEGs

In total, 1,452 DEGs (734 upregulated and 718 downregulated) were identified between the TP and DP groups (Fig. 2A). The DEGs were enriched in critical GO terms, including monocarboxylic metabolic processes, lipid metabolic processes, glycolytic processes, pyruvate metabolic processes, carboxylic acid metabolic processes, lipase activity, and other related processes

(Fig. 2B). Representative KEGG pathways included carbon metabolism, pyruvate metabolism, type II diabetes mellitus, AMPK signaling pathway, PPAR signaling pathway, citrate cycle, insulin signaling pathway, and other related processes (Fig. 2C).

Interaction network analysis of DEGs

We selected genes of the significantly enriched pathways in the functional enrichment analysis to construct a gene network diagram (Fig. 3). *ACACA* (acetyl-CoA carboxylase alpha), *SCD* (stearoyl-CoA desaturase), *LPIN1* (lipin 1), *HK1* (hexokinase 1), *FASN* (fatty acid synthase), *ACSS2* (acyl-CoA synthetase short-chain family member 2), *PCK2* (phosphoenolpyruvate carboxykinase 2), *ACLY* (ATP citrate lyase), *DLAT* (dihydrolipoamide S-acetyltransferase), *ALDOC* (aldolase, fructose-bisphosphate C), *LDHA* (lactate dehydrogenase A), and *ME1* (malic enzyme 1) interacted with each other. *ACACA*, *SCD*, *LPIN1*, and *HK1* strongly interacted in this network. Except for *LPIN1* and *PCK2*, which were downregulated, the other genes were upregulated in TPs. *ACACA* and *PCK2* were found be primarily associated with pyruvate metabolism, metabolic pathways, and the AMPK, insulin, and glucagon signaling pathways. *SCD*, *ALDOC*, and *ME1* were associated with oxoacid, carboxylic acid, and organic acid metabolic processes. *HK1*, *ACSS2*, *DLAT*, and *ALDOC* were found to be involved in glycolysis/gluconeogenesis and carbon metabolism, while *ACLY* was found to be involved in metabolic pathways and the citrate (TCA) cycle. *LDHA* was found to be involved in pyruvate metabolism, metabolic pathways, and glucagon and hypoxia-inducible factor 1 (HIF-1) signaling pathways (Table III). Based on the functional annotation, these DEGs may play important roles in fat deposition in TPs.

Table III. Potential key DEGs and their functions related to fat deposition.

Gene symbol	Log-2FC	P value	Padj	Trend	Functional analysis
ACACA	2.397	2.68 E-55	5.28 E-52	Up regulated	Pyruvate metabolism, metabolic pathways, AMPK signaling pathway, insulin signaling pathway, glucagon signaling pathway
SCD	4.068	1.83 E-79	8.13 E-76	Up regulated	Monocarboxylic acid metabolic process, lipid metabolic process, oxoacid metabolic process, carboxylic acid metabolic process, organic acid metabolic process, metabolic pathways, AMPK signaling pathway, PPAR signaling pathway
LPIN1	-1.262	2.07E-17	2.93 E-15	Down regulated	Metabolic pathways
HK1	1.6234	4.97 E-25	1.66 E-22	Up regulated	Glycolysis / gluconeogenesis, carbon metabolism, type II diabetes mellitus, metabolic pathways, HIF-1 signaling pathway, carbohydrate digestion and absorption, insulin signaling pathway, fructose and mannose metabolism, galactose metabolism
FASN	3.027	2.12E-50	3.13 E-47	Up regulated	Metabolic pathways, AMPK signaling pathway, insulin signaling pathway
ACSS2	2.0206	2.84E-42	3.36 E-39	Up regulated	Glycolysis / gluconeogenesis, carbon metabolism, pyruvate metabolism, metabolic pathways
PCK2	-1.939	3.60 E-16	4.43 E-14	Down regulated	Glycolysis / gluconeogenesis, pyruvate metabolism, metabolic pathways, AMPK signaling pathway, PPAR signaling pathway, citrate cycle (TCA cycle), insulin signaling pathway, glucagon signaling pathway
ACLY	2.7689	6.32E-34	4.31 E-31	Up regulated	Metabolic pathways, citrate cycle (TCA cycle)
DLAT	1.0568	3.03E-12	2.01 E-10	Up regulated	Glycolysis / gluconeogenesis, carbon metabolism, pyruvate metabolism, metabolic pathways, citrate cycle (TCA cycle)
ALDOC	2.3494	0.0013	0.009	Up regulated	Monocarboxylic acid metabolic process, ATP generation from ADP, glycolytic process, pyruvate metabolic process, oxoacid metabolic process, carboxylic acid metabolic process, organic acid metabolic process, ADP metabolic process, purine ribonucleoside diphosphate metabolic process, carbohydrate catabolic process, purine-containing compound metabolic process, glycolysis / gluconeogenesis, carbon metabolism, metabolic pathways, HIF-1 signaling pathway, biosynthesis of amino acids, fructose and mannose metabolism
LDHA	1.6334	1.08 E-17	1.63 E-15	Up regulated	Glycolysis / gluconeogenesis, pyruvate metabolism, metabolic pathways, HIF-1 signaling pathway, glucagon signaling pathway
ME1	1.667	3.84 E-11	2.05 E-09	Up regulated	oxoacid metabolic process, carboxylic acid metabolic process, organic acid metabolic process, carbon metabolism, pyruvate metabolism, metabolic pathways, PPAR signaling pathway

Padj represents the corrected *P* value.

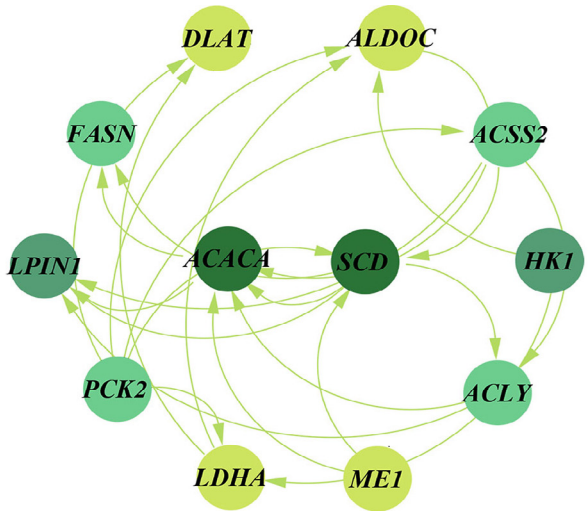

Fig. 3. Interaction network diagram of DEGs. Darker colors indicate stronger interactions.

Protein identification and quantification

A total of 580,244 spectra were obtained from 8PLEX LC-MS/MS analysis. Of the 25,492 peptides obtained, 19,397 unique peptides corresponding to 3,513 proteins were identified (Fig. 4A). The lengths of the peptides were mainly distributed between 7 and 25 amino acid residues, with peptides of 8 to 14 amino acids (AAs) being most abundant (Fig. 4B). The molecular weight of the proteins was mainly between 10 and 70 kDa (Fig. 4C). The proportion of proteins with a variation coefficient < 20% was > 90%, demonstrating good biological reproducibility within the group (Fig. 4D).

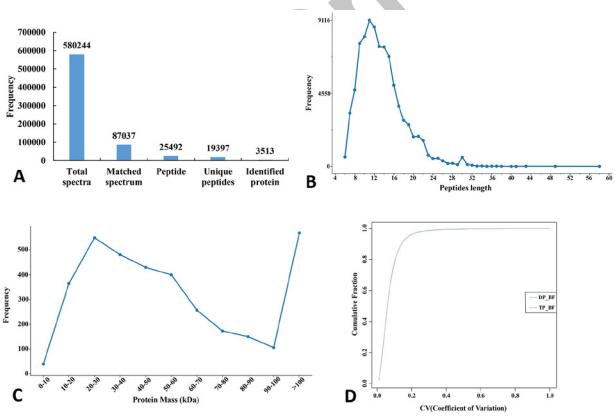

Fig. 4. Overview of protein identification information. (**A**) Basic information on protein identification. (**B**) Distribution of peptide lengths. (**C**) Distribution of the molecular weight classes of identified proteins. (**D**) The coefficient of variation (CV) of proteins in the replicates of the two groups.

Identification and functional analysis of DAPs

Comparison of protein profiles between TP and DP detected 126 DAPs, including 86 upregulated and 40 downregulated proteins (Fig. 5A). The DAPs were classified into two groups with good uniformity within the groups and distinct diversity between the two groups, indicating that the selected DAPs were relatively accurate (Fig. 5B).

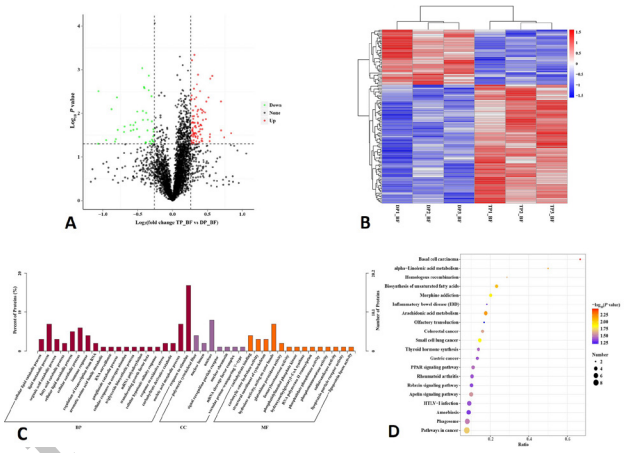

Fig. 5. Identification and functional analysis of DAPs. (**A**) Volcano plot displaying DAPs between TP and DP. Upregulated and downregulated genes are shown in red and green, respectively. Black dots represent genes with similar expression levels. (**B**) Heat map of DAPs. (**C**) GO enrichment analysis of DAPs between TP and DP. The x-axis displays GO enrichment terms, and the y-axis represents protein abundance. (**D**) KEGG enrichment analysis of DAPs between TP and DP. The x-axis shows ratio, and the y-axis represents KEGG enrichment terms. DP, Duroc pig; TP large Diqing Tibetan pig; BF, backfat.

Functional annotation of the 126 DAPs revealed GO terms primarily associated with lipid metabolic processes, fatty acid catabolic processes, cellular lipid metabolic processes, aromatic amino acid family metabolism, carbohydrate derivative catabolism, carbohydrate binding, and other related processes (Fig. 5C). The enriched representative KEGG pathways mainly included alpha-linolenic acid metabolism, biosynthesis of unsaturated FAs, arachidonic acid metabolism, thyroid hormone synthesis, and PPAR signaling pathway (Fig. 5D).

PPI network analysis

A total of 126 DAPs were used to construct a PPI network (Fig. 6). Proteins interacting in the network included SMAD2 (SMAD family member 2), ACTR10 (actin-related protein 10), HSPA4 (heat shock protein family A member 4), CTNNB1 (catenin beta 1), LCP1 (lymphocyte cytosolic protein 1), APOA4 (apolipoprotein

A4), TPM1 (tropomyosin 1), TTC36 (tetratricopeptide repeat domain 36), COL1A1 (collagen type I alpha 1 chain), HMGCS1 (3-hydroxy-3-methylglutaryl-CoA synthase 1), PARP1 (poly (ADP-ribose) polymerase 1), and SCD (stearoyl-CoA desaturase). SMAD2 and ACTR10 proteins interacted strongly in the network. APOA4, TPM1, and COL1A1 were downregulated whereas the other proteins were upregulated in TPs. SMAD2 was mainly associated with the FoxO, TGF-β, and apelin signaling pathways. HSPA4 was found to be involved in tight junctions, antigen processing, and antigen presentation. CTNNB1 was found to be associated with the Rap1, Wnt, and Hippo signaling pathways. LCP1, TTC36, and COL1A1 were found to be involved in protein binding, while APOA4 was involved in lipid transport, lipid binding, lipoprotein metabolism, and fat digestion and absorption. Furthermore, SCD was found to be associated with lipid metabolic processes, oxidation-reduction processes, biosynthesis of unsaturated FAs, fatty acid metabolism, PPAR signaling pathway, and AMPK signaling pathway (Table IV). These seven DAPs may play an important role in TP fat deposition.

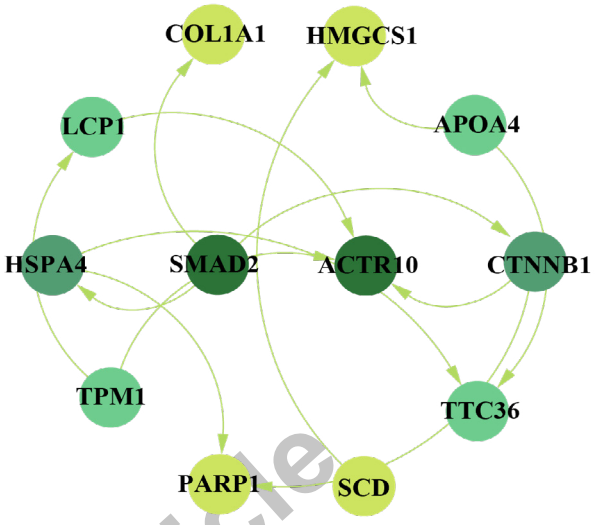

Fig. 6. Interaction network diagram of DAPs. Darker colors indicate stronger interactions.

Table IV. Potential key DAPs and their functions related to fat deposition.

Protein	P-value	Log2FC	Trend	Functional analysis
SMAD2	0.00138451	0.570593258	up	Intracellular, transcription factor complex, transforming growth factor beta receptor signaling pathway, FoxO signaling pathway, cell cycle, endocytosis, cellular senescence, TGF-beta signaling pathway, apelin signaling pathway, hippo signaling pathway, adherens junction, signaling pathways regulating pluripotency of stem cells, Th17 cell differentiation, relaxin signaling pathway, AGE-RAGE signaling pathway in diabetic complications
ACTR10	0.016266065	0.362776587	up	Actin-related protein 10
HSPA4	0.025959905	0.289588256	up	Tight junction, antigen processing and presentation
CTNNB1	0.029618982	0.339002742	up	Signal transducer activity, protein binding, adherens junction assembly, Rap1 signaling pathway, Wnt signaling pathway, hippo signaling pathway, focal adhesion, adherens junction, signaling pathways regulating pluripotency of stem cells, leukocyte transendothelial migration, thyroid hormone signaling pathway
LCP1	0.033688649	0.362081212	up	Calcium ion binding, protein binding
APOA4	0.043225782	-0.286167619	down	Extracellular region, lipid transport, lipid binding, lipoprotein metabolic process, fat digestion and absorption, vitamin digestion and absorption, cholesterol metabolism
TPM1	0.024568624	-0.360440878	down	Cardiac muscle contraction, adrenergic signaling in cardiomyocytes
TTC36	0.004735265	0.27125865	up	Protein binding
COL1A1	0.044521949	-0.823645222	down	Extracellular matrix structural constituent, protein binding
HMGCS1	0.029764693	0.31061633	up	Hydroxymethylglutaryl-CoA synthase activity, isoprenoid biosynthetic process, synthesis and degradation of ketone bodies, valine, leucine and isoleucine degradation, butanoate metabolism, terpenoid backbone biosynthesis, metabolic pathways
PARP1	0.011686944	0.288179702	up	DNA binding, NAD+ ADP-ribosyltransferase activity, protein ADP-ribosylation, zinc ion binding, base excision repair, apoptosis, necroptosis
SCD	0.005355015	0.693949206	up	lipid metabolic process, oxidation-reduction process, biosynthesis of unsaturated fatty acids, fatty acid metabolism, PPAR signaling pathway, AMPK signaling pathway

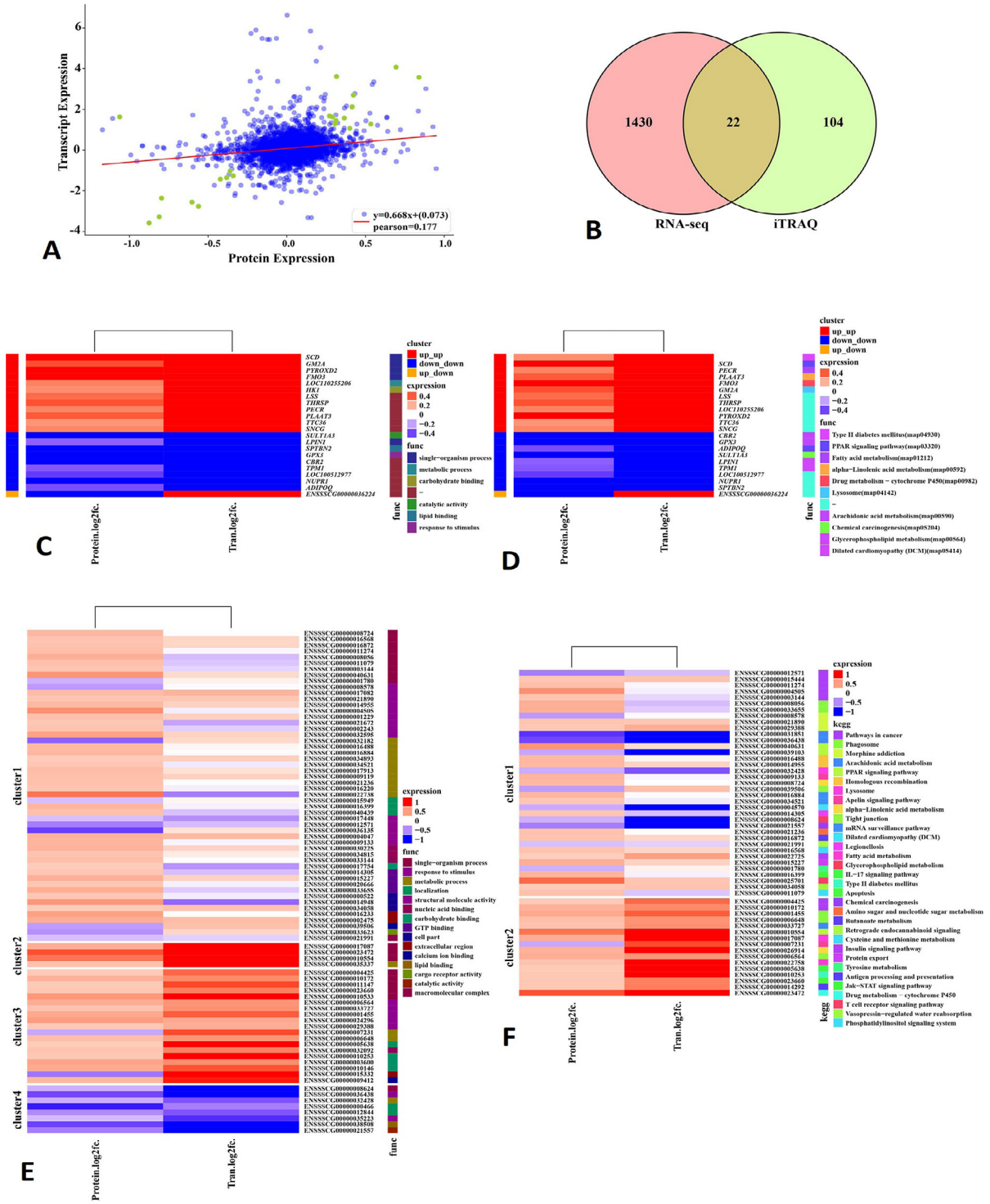

Fig. 7. Integrated analysis of iTRAQ and RNA-seq data. (**A**) The Pearson correlation coefficient of the fold changes of TP/DP between the mRNA and protein expression levels. The x-axis shows protein expression, and the y-axis represents transcript expression. (**B**) Venn diagram of the number of DAPs and DEGs. (**C**) Shared GO enrichment analysis of the 22 overlapping DEGs/DAPs. (**D**) Shared KEGG enrichment analysis of the 22 overlapping DEGs/DAPs. (**E**) GO enrichment heatmap of DAPs and DEGs. (**F**) KEGG enrichment heatmap of DAPs and DEGs.

Integrated analysis of iTRAQ and RNA-seq data

On integrating the 10,274 genes detected by RNA-seq and 3,513 proteins detected via iTRAQ, the Pearson correlation coefficient of the FCs of TP/DP between the mRNA and protein expression levels was found to be 0.073 (Fig. 7A). Among the 1,452 DEGs identified by RNA-seq and 126 DAPs via iTRAQ, 22 genes and proteins (*CBR2*, *TPM1*, *PECR*, *GPX3*, *PLAAT3*, *GM2A*, *LOC100512977*, *NUPR1*, *HK1*, *ENSSSCG00000036224*, *THRSP*, *LPIN1*, *SNCG*, *LSS*, *FMO3*, *SULT1A3*, *LOC110255206*, *SCD*, *PYROXD2*, *ADIPOQ*, *TTC36*, and *SPTBN2*) overlapped (Fig. 7B). The shared DEGs and DAPs were associated with metabolic processes, carbohydrate binding, catalytic activity, lipid binding, PPAR signaling pathway, fatty acid metabolism, and glycerophospholipid metabolism (Fig. 7C, D). The DEGs and DAPs were mainly related to GO terms for single-organism processes, responses to stimuli, metabolic processes, localization, structural molecule activity, nucleic acid binding, carbohydrate binding, GTP binding, cell part, extracellular region, calcium ion binding, lipid binding, cargo receptor activity, catalytic activity, and macromolecular complexes (Fig. 7E). The enriched KEGG pathways for the DEGs and DAPs were mainly pathways in cancer, phagosome, morphine addiction, arachidonic acid metabolism, PPAR signaling pathway, homologous recombination, lysosome, apelin signaling pathway, alpha-linolenic acid metabolism, tight junction, mRNA surveillance pathway, dilated cardiomyopathy (DCM), legionellosis, fatty acid metabolism, glycerophospholipid metabolism, IL-17 signaling pathway, type II diabetes mellitus, apoptosis, chemical carcinogenesis, amino sugar and nucleotide sugar metabolism, butanoate metabolism, retrograde endocannabinoid signaling, cysteine and methionine metabolism, insulin signaling pathway, protein export, tyrosine metabolism, antigen processing and presentation, JAK-STAT signaling pathway, drug metabolism-cytochrome P450, T-cell receptor signaling pathway, vasopressin-regulated water reabsorption, and phosphatidylinositol signaling system (Fig. 7F).

Validation of DEGs

Six DEGs (*ACACA*, *PLAAT3*, *SCD*, *SREBF1*, *THRSP*, and *ADIPOQ*) were selected to validate expression differences by RNA-seq using qPCR. The expression of genes in the TP vs. DP group was consistent with the results of transcriptome sequencing (Fig. 8). These results indicate the reliable and efficient identification of DEGs by RNA-seq.

DISCUSSION

The current study screened for key genes and proteins related to fat deposition by comparing gene and protein profiles of TPs and DPs raised under the same feeding conditions, using RNA-seq and iTRAQ protein sequencing analyses, respectively. Subsequent functional enrichment analysis of each DEG and DAP identified via these analyses using GO and KEGG analysis identified 22 DEGs and DAPs (*CBR2*, *TPM1*, *PECR*, *GPX3*, *PLAAT3*, *GM2A*, *LOC100512977*, *NUPR1*, *HK1*, *ENSSSCG00000036224*, *THRSP*, *LPIN1*, *SNCG*, *LSS*, *FMO3*, *SULT1A3*, *LOC110255206*, *SCD*, *PYROXD2*, *ADIPOQ*, *TTC36*, and *SPTBN2*) with potential roles in fat deposition.

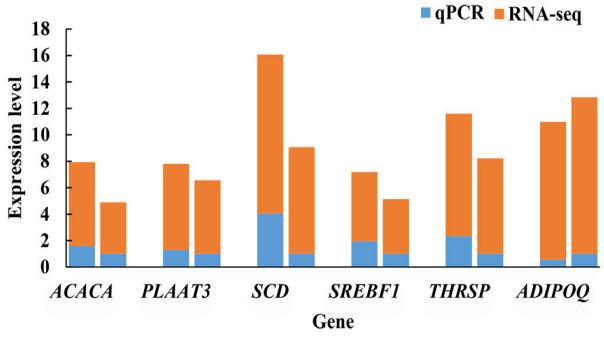

Fig. 8. qPCR results of DEGs. The x-axis shows gene symbols, and the y-axis represents expression. Orange represents RNA-seq data and blue represents qPCR data.

Fat deposition in adipose tissue is a complex metabolic process involving many genes and includes the growth and deposition of fat. The deposition of fat occurs in the late growth stage. The present results support the status of adipocytes as highly complex cells with important role in various metabolic processes. Carbohydrate metabolism is an important component of energy and lipid metabolism. It is upstream of de novo FA synthesis and can supply substrates for FA (Xing *et al*., 2019). This study identified six DEGs (*SCD*, *LPIN1*, *PECR*, *FMO3*, *THRSP*, and *SNCG*) and corresponding DAPs associated with pyruvate metabolism, lipid metabolism, FA synthesis, FA metabolism, FA oxidation, adipocyte differentiation, and adipogenesis. *SCD* belongs to the FA desaturase family, which encodes an enzyme involved in FA biosynthesis, mainly promoting oleic acid synthesis. The expression of the *SCD* gene can increase FA desaturation and intramuscular fat content (Fernández *et al*., 2017). Two subtypes of *SCD* have been identified, *SCD1* and *SCD5*. In humans, high activity of *SCD* results in the accumulation and storage of triglycerides in the liver. The porcine *SCD1* gene located on chromosome 14 (Ren *et al*., 2003) is mainly expressed in adipose tissue,

liver, and muscle. *SCD1* deficiency increases systemic glucose uptake, and liver *SCD1* deficiency promotes the expression of glucose transporter 1 in the liver and upregulates the expression of glutamine 4 and adiponectin in adipose tissue (Aljohani *et al*., 2019). At the individual level, *SCD1* full-gene knockout mice feature accelerated energy metabolism, which is characterized by increased lipid oxidation, decreased synthesis, enhanced insulin sensitivity, resistance to obesity, and FA degeneration induced by high-carbohydrate and high-fat diets (Ntambi *et al*., 2002). *LPIN1* is necessary for adipocyte differentiation. The encoded enzyme catalyzes triglyceride synthesis, and is essential for normal adipose tissue development (He *et al*., 2009). LPIN1 is a bifunctional protein that serves as a nuclear transcriptional coactivator in hepatocytes, where it interacts with a complex containing PPARα and PPARγ coactivator-1α (PGC-1α) to regulate the expression of genes involved in FA oxidation. In addition, Phan and Reue (2005) found that LPIN1 suppressed FA oxidation under normal glucose conditions (25 mM) and promoted FA oxidation under low-glucose conditions (1 mM) in C2C12 myoblasts. Peroxisomal trans-2-enoyl-CoA reductase (PECR), also termed truncated estrogen receptor product (TERP) and trans-2,3-enoyl-CoA reductase (TECR), can participate in carbon chain elongation in FA metabolism and catalyze the last reaction of four long-chain FA elongation cycles (Wakashima *et al*., 2014). PECR is a peroxisomal protein involved in FA synthesis and metabolic pathways. The protein is expressed in smooth muscle, kidneys, liver, and adipocytes. Abe *et al*. (2013) reported that *PECR* plays an important role in the late synthesis of triglycerides (TGs) and in the treatment of fatty diseases. *PECR* micro RNAs (miRNAs) can participate in FA metabolism and unsaturated FAs biosynthesis. Rasooly *et al*. (2007) demonstrated downregulation of the *cyt P450* and *FMO3* genes by feeding diets containing conjugated linoleic acid preparations to mouse which detected by microarray chips, which are involved in the ω hydroxylation of FAs and the production of dicarboxylic FAs. Once formed, dicarboxylic FAs can be shortened from either end of the molecule by β-oxidation. This pathway plays a significant role in FA oxidation during starvation and diabetes. Thyroid hormone response point 14 (*THRSP*) mainly exists in the nucleus of adipose tissue, adipocytes, and related cells in muscle and cells of the hepatic portal vein triad, and is expressed in mature adipocytes, rather than in the early stages of adipogenesis (Schering *et al*., 2017). *THRSP* is involved in the transcriptional regulation of gene expression of various lipogenic rate-limiting enzymes. *THRSP* regulates its expression through polymorphism of transcription factors and promoter regions and affects adipogenesis (Wang *et al*., 2020). *SNCG* is a target gene involved in mediating metabolic function of adipocytes. Notably, *SNCG* supports adipocyte differentiation and adipose tissue expansion, and its functions are particularly important under conditions of nutrient excess (Oort *et al*., 2008). These findings demonstrate a novel mechanism by which homeostatic miRNAs found in adipose tissue may serve as key rheostats, modulating impaired adipogenesis and fat mass expansion through the control of *SNCG*. Millership *et al*. (2012) defined the specific role of *SNCG* in fat mass expansion in *SNCG*-null mice administered a high-fat diet. They observed that the loss of *SNCG* protects against the development of diet-induced obesity while ameliorating obesity-related hyperinsulinemia and hepatosteatosis.

The amount of fat deposition is affected by the synthesis of FAs and by the metabolism and oxidation of fat. Adipocytes are not only passive fat deposits but are also important in maintaining energy balance and homeostasis in the body. Adipose tissue acts as a receptor for lipid levels, transmitting information to the neural circuits that regulate hunger and satiety. *PPARs* are members of the nuclear receptor family that regulate energy balance, fat metabolism, cell differentiation, and proliferation through the speech signaling pathway. Activation of the PPAR signaling pathway promotes FA oxidation. PLAAT protein was the first mammalian enzyme reported to show N-acyltransferase activity. The enzyme catalyzes the formation of N-acylethanolamine phospholipids from ethanolamine phospholipids (Ueda *et al*., 2013). We have previously described that overexpression of *PLAAT3* in animal cells resulted in the disappearance of peroxisomes and a remarkable reduction in plasmalogen levels, indicating the possibility that PLAAT protein regulates plasmalogen levels through peroxisome biogenesis (Uyama *et al*., 2012). *PLAAT3* has been identified as a PPAR-γ target gene. Compared with wild-type mice, white adipose tissue of *PLAAT3*-deficient mice contained significantly smaller adipocytes, and their triacylglycerol levels decreased. When PLAAT-3 is deficient, cAMP levels rise, resulting in a high lipolysis rate (Uyama *et al*., 2017). Mechanistically, *NUPR1* participates in the activation of PPAR-α signaling via the unfolded protein response (UPR). As PPAR-α signaling is controlled by the UPR, collectively, these findings suggest a novel function for *NUPR1* in controlling lipid homeostasis, possibly through the UPR (Teresa Borrello *et al*., 2021).

In the present study, *GM2A*, *HK1*, and *ADIPOQ* were found to be involved in the insulin signaling pathway and insulin resistance. *GM2A* is associated with insulin resistance, decreasing insulin sensitivity, which decreased lipolysis and promoted adipogenesis (Kirby *et al*., 2016). *HK1* participates in the metabolism of starch and sucrose, phosphorylates glucose to produce glucose-6-phosphate, and then induces glucose-reactive insulin

secretion (Frantz *et al*., 2013). *ADIPOQ* is expressed only in adipose tissue and activates AMP-activated protein kinase (AMPK) and PPARα by improving systemic insulin resistance, reducing glucose production, increasing the utilization of glucose and FAs in skeletal muscle, and reducing blood glucose levels (Yanai and Yoshida, 2019). Adiponectin concentration is related to lipoprotein metabolism, particularly high-density lipoprotein (HDL) and triglyceride metabolism. Adiponectin can increase HDL levels and reduce triglyceride levels. It can also inhibit glucose production by reducing the availability of glucose-producing substrates. Adiponectin stimulates FA oxidation, thereby reducing glucose production. Adiponectin also has a synergistic effect on leptin levels. Adiponectin, leptin, and FAs maintain metabolic homeostasis through adipose tissue crosstalk (Stern *et al*., 2016). When excessive fat deposition occurs in animals, the expression of *ADIPOQ* and *ADIPOQ* levels in the blood decrease accordingly. When insulin resistance is induced, fat cells and muscle cells exhibit an insufficient response to normal insulin concentrations, which reduces insulin sensitivity, promotes glucose uptake and utilization efficiency, results in excessive energy intake, and reduces lipolysis (Kim *et al*., 2017). Furthermore, adiponectin can activate AMPK, reduce the production of malonyl C_0A, and promote the oxidation of FAs in mitochondria (Bu *et al*., 2012). When adiponectin resistance occurs, AMPK stimulation by adiponectin is weakened, and the effect of FA oxidation in skeletal muscle is weakened, thus promoting insulin resistance.

CONCLUSION

This study identified crucial genes and proteins involved in fat deposition in TPs by combining RNA-seq and iTRAQ data obtained from pig BF tissues. The findings elucidate the regulatory relationship between DEGs and DAPs. A combination of transcriptomic and proteomic data revealed several key candidate regulators (*SCD*, *LPIN1*, and *HK1*) and pathways (metabolic processes, insulin signaling pathway, and fatty acid synthesis) that might be crucial in the fat deposition traits of TPs. The study findings provide a reference for analyzing the genetic regulatory mechanisms of fat deposition in pigs to improve the meat quality of TPs by molecular marker-assisted selection.

DECLARATIONS

Acknowledgment

This study was funded by the Yunnan Agricultural Basic Research Joint Project (202101BD070001-103), Major Science and Technology Projects in Yunnan Province (202202AE090005) and Major Science and Technology Projects in Yunnan Province (202302AE090015).

Ethical approval

This study was conducted under the approval and instructions of the Ethics Committee of Yunnan Agriculture University (Permit number: 20211003) and the animal ethics requirements of the People's Republic of China.

Statement of conflicts of interest

The authors have declared no conflict of interest.

REFERENCES

Abe, K., Ohno, Y., Sassa, T., Taguchi, R., Caliskan, M., Ober, C. and Kihara, A., 2013. Mutation for nonsyndromic mental retardation in the trans-2-enoyl-CoA reductase TER gene involved in fatty acid elongation impairs the enzyme activity and stability, leading to change in sphingolipid profile. *J. biol. Chem*., **288**: 36741-36749. https://doi.org/10.1074/jbc.M113.493221

Aljohani, A., Khan, M.I., Bonneville, A., Guo, C., Jeffery, J., O'Neill, L., Syed, D.N., Lewis, S.A., Burhans, M. and Mukhtar, H., 2019. Hepatic stearoyl CoA desaturase 1 deficiency increases glucose uptake in adipose tissue partially through the PGC-1α–FGF21 axis in mice. *J. biol. Chem*., **294**: 19475-19485. https://doi.org/10.1074/jbc.RA119.009868

Anders, S. and Huber, W., 2010. Differential expression analysis for sequence count data. *Genome Biol*., **11**: R106. https://doi.org/10.1186/gb-2010-11-10-r106

Bowers, R.R., Kim, J.W., Otto, T.C. and Lane, M.D., 2006. Stable stem cell commitment to the adipocyte lineage by inhibition of DNA methylation: Role of the BMP-4 gene. *Proc. natl. Acad. Sci. U.S.A*., **103**: 13022-13027. https://doi.org/10.1073/pnas.0605789103

Bu, J., Feng, Q., Ran, J., Li, Q., Mei, G. and Zhang, Y., 2012. Visceral fat mass is always, but adipokines (adiponectin and resistin) are diversely associated with insulin resistance in Chinese type 2 diabetic and normoglycemic subjects. *Diabetes Res. Clin. Pract*., **96**: 163-169. https://doi.org/10.1016/j.diabres.2011.12.014

Cardoso, T.F., Canovas, A., Canela-Xandri, O., Gonzalez-Prendes, R., Amills, M. and Quintanilla, R., 2017. RNA-seq based detection of differentially expressed genes in the skeletal muscle of Duroc pigs with distinct lipid profiles. *Sci. Rep*., **7**: 40005.

https://doi.org/10.1038/srep40005

Chen, W., Fang, G.F., Wang, S.D., Wang, H. and Zeng, Y.Q., 2017. Longissimus lumborum muscle transcriptome analysis of Laiwu and Yorkshire pigs differing in intramuscular fat content. *Genes Genom.*, **39**: 759-766. https://doi.org/10.1007/s13258-017-0540-9

Corominas, J., Ramayo-Caldas, Y., Puig-Oliveras, A., Estelle, J., Castello, A., Alves, E., Pena, R.N., Ballester, M. and Folch, J.M., 2013. Analysis of porcine adipose tissue transcriptome reveals differences in de novo fatty acid synthesis in pigs with divergent muscle fatty acid composition. *BMC Genomics*, **14**: 843. https://doi.org/10.1186/1471-2164-14-843

Davis, L.A. and Zur Nieden, N.I., 2008. Mesodermal fate decisions of a stem cell: The Wnt switch. *Cell Mol. Life Sci.*, **65**: 2658-2674. https://doi.org/10.1007/s00018-008-8042-1

Eggert, J., Grant, A. and Schinckel, A., 2007. Factors affecting fat distribution in pork carcasses. *Prof. Anim. Sci.*, **23**: 42-53. https://doi.org/10.1532/S1080-7446(15)30935-9

Fernández, A.I., Óvilo, C., Barragán, C., Rodríguez, M.C., Silió, L., Folch, J.M. and Fernández, A., 2017. Validating porcine SCD haplotype effects on fatty acid desaturation and fat deposition in different genetic backgrounds. *Livest. Sci.*, **205**: 98-105. https://doi.org/10.1016/j.livsci.2017.09.021

Frantz, E.D., Crespo-Mascarenhas, C., Barreto-Vianna, A.R., Aguila, M.B. and Mandarim-de-Lacerda, C.A., 2013. Renin-angiotensin system blockers protect pancreatic islets against diet-induced obesity and insulin resistance in mice. *PLoS One*, **8**: e67192. https://doi.org/10.1371/journal.pone.0067192

Ge, Q., Gao, C., Cai, Y., Jiao, T., Quan, J., Guo, Y., Zheng, W. and Zhao, S., 2020. Evaluating genetic diversity and identifying priority conservation for seven Tibetan pig populations in China based on the mtDNA D-loop. *Asian-Austral. J. Anim. Sci.*, **33**: 1905-1911. https://doi.org/10.5713/ajas.19.0752

Hausman, G.J., Bergen, W.G., Etherton, T.D. and Smith, S.B., 2018. The history of adipocyte and adipose tissue research in meat animals. *J. Anim. Sci.*, **96**: 473-486. https://doi.org/10.1093/jas/skx050

He, X., Xu, X., Zhao, S., Fan, B., Yu, M., Zhu, M., Li, C., Peng, Z. and Liu, B., 2009. Investigation of Lpin1 as a candidate gene for fat deposition in pigs. *Mol. Biol. Rep.*, **36**: 1175-1180. https://doi.org/10.1007/s11033-008-9294-4

Huang, W., Zhang, X., Li, A., Xie, L. and Miao, X., 2017. Differential regulation of mRNAs and lncRNAs related to lipid metabolism in two pig breeds. *Oncotarget*, **8**: 87539-87553. https://doi.org/10.18632/oncotarget.20978

Jia, C., Kong, X., Koltes, J.E., Gou, X., Yang, S., Yan, D., Lu, S. and Wei, Z., 2016. Gene co-expression network analysis unraveling transcriptional regulation of high-altitude adaptation of tibetan pig. *PLoS One*, **11**: e0168161. https://doi.org/10.1371/journal.pone.0168161

Kim, J.Y., Nasr, A., Tfayli, H., Bacha, F., Michaliszyn, S.F. and Arslanian, S., 2017. Increased lipolysis, diminished adipose tissue insulin sensitivity, and impaired β-cell function relative to adipose tissue insulin sensitivity in obese youth with impaired glucose tolerance. *Diabetes*, **66**: 3085-3090. https://doi.org/10.2337/db17-0551

Kirby, T.J., Walton, R.G., Finlin, B., Zhu, B., Unal, R., Rasouli, N., Peterson, C.A. and Kern, P.A., 2016. Integrative mRNA-microRNA analyses reveal novel interactions related to insulin sensitivity in human adipose tissue. *Physiol. Genomics*, **48**: 145-153. https://doi.org/10.1152/physiolgenomics.00071.2015

Lee, Y.B. and Kauffman, R.G., 1974. Cellular and enzymatic changes with animal growth in porcine intramuscular adipose tissue. *J. Anim. Sci.*, **38**: 532-537. https://doi.org/10.2527/jas1974.383532x

Li, H., Handsaker, B., Wysoker, A., Fennell, T., Ruan, J., Homer, N., Marth, G., Abecasis, G., Durbin, R. and Genome Project Data Processing, S., 2009. The sequence alignment/map format and SAMtools. *Bioinformatics*, **25**: 2078-2079. https://doi.org/10.1093/bioinformatics/btp352

Lin, C.S., Xin, Z.C., Deng, C.H., Ning, H., Lin, G. and Lue, T.F., 2010. Defining adipose tissue-derived stem cells in tissue and in culture. *Histol, Histopathol.*, **25**: 807-815.

Michalski, A., Damoc, E., Hauschild, J.P., Lange, O., Wieghaus, A., Makarov, A., Nagaraj, N., Cox, J., Mann, M. and Horning, S., 2011. Mass spectrometry-based proteomics using Q exactive, a high-performance benchtop quadrupole Orbitrap mass spectrometer. *Mol. Cell. Proteomics*, **10**: M111 011015. https://doi.org/10.1074/mcp.M111.011015

Millership, S., Ninkina, N., Guschina, I.A., Norton, J., Brambilla, R., Oort, P.J., Adams, S.H., Dennis, R.J., Voshol, P.J. and Rochford, J.J., 2012. Increased lipolysis and altered lipid homeostasis protect γ-synuclein–null mutant mice from diet-induced obesity. *Proc. natl. Acad. Sci.*, **109**: 20943-20948.

https://doi.org/10.1073/pnas.1210022110

Monziols, M., Bonneau, M., Davenel, A. and Kouba, M., 2007. Comparison of the lipid content and fatty acid composition of intermuscular and subcutaneous adipose tissues in pig carcasses. *Meat Sci*., **76**: 54-60. https://doi.org/10.1016/j.meatsci.2006.10.013

Muñoz, M., García-Casco, J.M., Caraballo, C., Fernández-Barroso, M.Á., Sánchez-Esquiliche, F., Gómez, F., Rodriguez, M.D.C. and Silió, L., 2018. Identification of candidate genes and regulatory factors underlying intramuscular fat content through longissimus dorsi transcriptome analyses in heavy Iberian pigs. *Front. Genet*., **9**: 608. https://doi.org/10.3389/fgene.2018.00608

Ntambi, J.M., Miyazaki, M., Stoehr, J.P., Lan, H., Kendziorski, C.M., Yandell, B.S., Song, Y., Cohen, P., Friedman, J.M. and Attie, A.D., 2002. Loss of stearoyl-CoA desaturase-1 function protects mice against adiposity. *Proc. natl. Acad. Sci. U.S.A*., **99**: 11482-11486. https://doi.org/10.1073/pnas.132384699

Oort, P.J., Knotts, T.A., Grino, M., Naour, N., Bastard, J.P., Clément, K., Ninkina, N., Buchman, V.L., Permana, P.A. and Luo, X., 2008. γ-synuclein is an adipocyte-neuron gene coordinately expressed with leptin and increased in human obesity. *J. Nutr*., **138**: 841-848. https://doi.org/10.1093/jn/138.5.841

Pan, P., Zhao, S., Yu, M., Liu, B., Xiong, T. and Li, K., 2003. Identification of differentially expressed genes in the longissimus dorsi muscle tissue between duroc and erhualian pigs by mRNA differential display. *Asian-Australas. J. Anim. Sci*., **16**: 1066-1070. https://doi.org/10.5713/ajas.2003.1066

Phan, J. and Reue, K., 2005. Lipin, a lipodystrophy and obesity gene. *Cell Metab*., **1**: 73-83. https://doi.org/10.1016/j.cmet.2004.12.002

Rasooly, R., Kelley, D.S., Greg, J. and Mackey, B.E., 2007. Dietary trans 10, cis 12-conjugated linoleic acid reduces the expression of fatty acid oxidation and drug detoxification enzymes in mouse liver. *Br. J. Nutr*., **97**: 58-66. https://doi.org/10.1017/S0007114507257745

Ren, J., Knorr, C., Habermann, F., Fries, R., Huang, L.S. and Brenig, B., 2003. Assignment of the porcine stearoyl-CoA desaturase (SCD) gene to SSC14q27 by fluorescence in situ hybridization and by hybrid panel mapping. *Anim. Genet*., **34**: 471-473. https://doi.org/10.1046/j.0268-9146.2003.01058.x

Sandberg, A., Lindell, G., Kallstrom, B.N., Branca, R.M., Danielsson, K.G., Dahlberg, M., Larson, B., Forshed, J. and Lehtio, J., 2012. Tumor proteomics by multivariate analysis on individual pathway data for characterization of vulvar cancer phenotypes. *Mol. Cell Proteom.*, **11**: M112 016998. https://doi.org/10.1074/mcp.M112.016998

Schering, L., Albrecht, E., Komolka, K., Kühn, C. and Maak, S., 2017. Increased expression of thyroid hormone responsive protein (THRSP) is the result but not the cause of higher intramuscular fat content in cattle. *Int. J. biol. Sci*., **13**: 532. https://doi.org/10.7150/ijbs.18775

Sodhi, S.S., Park, W.C., Ghosh, M., Kim, J.N., Sharma, N., Shin, K.Y., Cho, I.C., Ryu, Y.C., Oh, S.J., Kim, S.H., Song, K.D., Hong, S.P., Cho, S.A., Kim, H.B. and Jeong, D.K., 2014. Comparative transcriptomic analysis to identify differentially expressed genes in fat tissue of adult Berkshire and Jeju Native Pig using RNA-seq. *Mol. Biol. Rep*., **41**: 6305-6315. https://doi.org/10.1007/s11033-014-3513-y

Spinella-Jaegle, S., Rawadi, G., Kawai, S., Gallea, S., Faucheu, C., Mollat, P., Courtois, B., Bergaud, B., Ramez, V.R. and Blanchet, A.M., 2001. Sonic hedgehog increases the commitment of pluripotent mesenchymal cells into the osteoblastic lineage and abolishes adipocytic differentiation. *J. Cell Sci*., **114**: 2085-2094. https://doi.org/10.1242/jcs.114.11.2085

Stern, J.H., Rutkowski, J.M. and Scherer, P.E., 2016. Adiponectin, leptin, and fatty acids in the maintenance of metabolic homeostasis through adipose tissue crosstalk. *Cell Metab*., **23**: 770-784. https://doi.org/10.1016/j.cmet.2016.04.011

Tang, Q.Q. and Lane, M.D., 2012. Adipogenesis from stem cell to adipocyte. *Annu. Rev. Biochem*., **81**: 715-736. https://doi.org/10.1146/annurev-biochem-052110-115718

Teresa, B.M., Rita, E.M., Listi, A., Rubis, M., Coslet, S., Augello, G., Cusimano, A., Cabibi, D., Porcasi, R., Giannitrapani, L., Soresi, M., Pantuso, G., Blyth, K., Montalto, G., Pin, C., Cervello, M. and Iovanna, J., 2021. NUPR1 protects liver from lipotoxic injury by improving the endoplasmic reticulum stress response. *FASEB J*., **35**: e21395. https://doi.org/10.1096/fj.202002413RR

Trapnell, C., Pachter, L. and Salzberg, S.L., 2009. TopHat discovering splice junctions with RNA-Seq. *Bioinformatics*, **25**: 1105-1111. https://doi.org/10.1093/bioinformatics/btp120

Trapnell, C., Williams, B.A., Pertea, G., Mortazavi, A., Kwan, G., van Baren, M.J., Salzberg, S.L., Wold, B.J. and Pachter, L., 2010. Transcript assembly and quantification by RNA-Seq reveals unannotated transcripts and isoform switching during cell differentiation. *Nat. Biotechnol*., **28**: 511-515. https://doi.org/10.1038/nbt.1621

Ueda, N., Tsuboi, K. and Uyama, T., 2013.

Metabolism of endocannabinoids and related N-acylethanolamines: canonical and alternative pathways. *FEBS J*., **280**: 1874-1894. https://doi.org/10.1111/febs.12152

Uyama, T., Ichi, I., Kono, N., Inoue, A., Tsuboi, K., Jin, X.H., Araki, N., Aoki, J., Arai, H. and Ueda, N., 2012. Regulation of peroxisomal lipid metabolism by catalytic activity of tumor suppressor H-rev107. *J. biol. Chem*., **287**: 2706-2718. https://doi.org/10.1074/jbc.M111.267575

Uyama, T., Tsuboi, K. and Ueda, N., 2017. An involvement of phospholipase A/acyltransferase family proteins in peroxisome regulation and plasmalogen metabolism. *FEBS Lett*., **591**: 2745-2760. https://doi.org/10.1002/1873-3468.12787

Wakashima, T., Abe, K. and Kihara, A., 2014. Dual functions of the trans-2-enoyl-CoA reductase TER in the sphingosine 1-phosphate metabolic pathway and in fatty acid elongation. *J. biol. Chem*., **289**: 24736-24748. https://doi.org/10.1074/jbc.M114.571869

Wang, C., Liu, C.M., Wei, L.L., Shi, L.Y., Pan, Z.F., Mao, L.G., Wan, X.C., Ping, Z.P., Jiang, T.T., Chen, Z.L., Li, Z.J. and Li, J.C., 2016. A group of novel serum diagnostic biomarkers for multidrug-resistant tuberculosis by iTRAQ-2D LC-MS/MS and solexa sequencing. *Int. J. biol. Sci*., **12**: 246-256. https://doi.org/10.7150/ijbs.13805

Wang, T., Jiang, A., Guo, Y., Tan, Y., Tang, G., Mai, M., Liu, H., Xiao, J., Li, M. and Li, X., 2013. Deep sequencing of the transcriptome reveals inflammatory features of porcine visceral adipose tissue. *Int. J. biol. Sci*., **9**: 550-556. https://doi.org/10.7150/ijbs.6257

Wang, X., Cheng, J., Qin, W., Chen, H., Chen, G., Shang, X., Zhang, M., Balsai, N. and Chen, H., 2020. Polymorphisms in 5' proximal regulating region of THRSP gene are associated with fat production in pigs. *3 Biotech*, **10**: 267. https://doi.org/10.1007/s13205-020-02266-6

Wu, D.D., Yang, C.P., Wang, M.S., Dong, K.Z., Yan, D.W., Hao, Z.Q., Fan, S.Q., Chu, S.Z., Shen, Q.S. and Jiang, L.P., 2020. Convergent genomic signatures of high-altitude adaptation among domestic mammals. *Natl. Sci. Rev*., **7**: 952-963. https://doi.org/10.1093/nsr/nwz213

Xing, K., Wang, K., Ao, H., Chen, S., Tan, Z., Wang, Y., Xitong, Z., Yang, T., Zhang, F., Liu, Y., Ni, H., Sheng, X., Qi, X., Wang, X., Guo, Y. and Wang, C., 2019. Comparative adipose transcriptome analysis digs out genes related to fat deposition in two pig breeds. *Sci. Rep*., **9**: 12925. https://doi.org/10.1038/s41598-019-49548-5

Yanai, H. and Yoshida, H., 2019. Beneficial effects of adiponectin on glucose and lipid metabolism and atherosclerotic progression: Mechanisms and perspectives. *Int. J. mol. Sci*., **20**: 1190. https://doi.org/10.3390/ijms20051190

Yang, S., Zhang, H., Mao, H., Yan, D., Lu, S., Lian, L., Zhao, G., Yan, Y., Deng, W. and Shi, X., 2011. The local origin of the Tibetan pig and additional insights into the origin of Asian pigs. *PLoS One*, **6**: e28215. https://doi.org/10.1371/journal.pone.0028215